Soliton Model of Competitive Neural Dynamics during Binocular Rivalry

P. N. Loxley[1,2] and P. A. Robinson[1,2,3]

[1]School of Physics, The University of Sydney, Sydney, New South Wales 2006, Australia
[2]Brain Dynamics Center, Westmead Hospital, Westmead, New South Wales 2145, Australia
[3]Faculty of Medicine, The University of Sydney, Sydney, New South Wales 2006, Australia

(Received 23 September 2008; revised manuscript received 6 May 2009; published 23 June 2009)

Binocular rivalry is investigated in a continuum model of the primary visual cortex that includes neural excitation and inhibition, stimulus orientation preference, and spike-rate adaptation. Visual stimuli consisting of bars or edges result in localized states of neural activity described by solitons. Stability analysis shows binocular fusion gives way to binocular rivalry when the orientation difference between left-eye and right-eye stimuli destabilizes one or more solitons. The model yields conditions for binocular rivalry, and two types of competitive dynamics are found: either one soliton oscillates between two stimulus regions or two solitons fixed in position at the stimulus regions oscillate out of phase with each other.

DOI: 10.1103/PhysRevLett.102.258701 PACS numbers: 42.66.Si, 05.45.Yv, 87.10.Ed, 87.19.lj

Binocular rivalry occurs when we view certain dissimilar monocular stimuli, such as a series of horizontal bars with one eye and a series of vertical bars with the other. This leads to alternations in visual perception, where one eye's input dominates, then the other's [1,2]. A similar phenomenon occurs when viewing ambiguous figures such as the Necker cube [2], where two perceptual interpretations alternate over time. Binocular rivalry is linked to neural activity in the primary visual cortex (V1) [3,4], where neurons respond most strongly to visual stimuli such as a bar or edge of particular orientation [5]. This orientation preference (OP) changes smoothly across V1, except at isolated locations [5]. Visual stimuli consisting of bars or edges of specific orientation therefore activate specific groups of neurons in V1. Key elements in most neural models of visual rivalry include reciprocal inhibition and adaptation [6–9]: reciprocal inhibition takes place over fast time scales and involves neurons coupled so that when one set is active, another set is suppressed, while adaptation causes the active neurons to fatigue over slow time scales, allowing the suppressed neurons to become active. While current neural models successfully reproduce some key properties of binocular rivalry, such as the distribution of perceptual dominance durations [6,8,9], and the propagation of dominance changes across V1 [8], there are no clear predictions of what conditions trigger the breakdown of binocular fusion (where inputs to left and right eyes form a stable fused percept) and the onset of rivalry. It is also unclear what types of dynamics take place during rivalry, with some findings suggesting neural activity consists of traveling waves [4,8], and others that alternations in activity remain fixed in position [7,9].

In this Letter, we present a physiologically based continuum model of binocular rivalry that allows detailed investigation of the fusion-rivalry transition as stimulus parameters are varied and exhibits two types of competitive neural dynamics consistent with rivalry. For simplicity we consider a one-dimensional (1D) slice through V1, and calculate the activity $u(x, t)$ of neural populations coupled through a synaptic connectivity function $w(R)$ which depends on the distance R between neurons, and subject to a visual stimulus $h(x)$ that drives neural activity. The dynamical equations are

$$\mathcal{D}_f u(x,t) = \int_{-\infty}^{\infty} w(x-x')H(u(x',t)-\theta(x',t))dx' + h(x), \tag{1}$$

$$\mathcal{D}_s \theta(x,t) = \theta_0 + \kappa u(x,t) H(u(x,t)), \tag{2}$$

where $\mathcal{D}_a \equiv \tau_a \partial/\partial t + 1$, τ_a is a time constant, and H is the unit step function: satisfying $H(x) = 0$ if $x < 0$, and $H(x) = 1$ if $x \geq 0$. Equation (1) describes the fast process where incoming spikes are smoothed into pulses of duration τ_f at the synapses of a neuron [7,8,10]. The spiking rate of a neural population is assumed to follow a threshold response $H(u - \theta)$. Equation (2) describes slow processes which cause the spiking rate to adapt over time [7,8,11,12], and changes the spiking threshold $\theta(x, t)$ over a time scale $\tau_s \gg \tau_f$; $H(u)$ is used in (2) so the coupling is linear in u for $u > 0$, and zero for $u < 0$.

Visual stimuli consisting of bars or edges activate groups of neurons in V1 with OP near the stimulus orientation—some sensitive to left-eye stimuli, others to right-eye stimuli. Since OP varies across V1, stimuli of different orientations are mapped to different parts of V1 even when they are from the same point in the visual field. A typical 1D slice through V1 (see Fig. 1) that includes the full OP range 0°–180°, plus left-eye and right-eye stimulus preferences, contains the essential elements for a fusion-rivalry transition, and is consistent with the known structure of V1 [5]. Monocular stimuli are included in (1) using $h(x)/h_{\max} = e^{-(x+d/2)^2/\delta} + e^{-(x-d/2)^2/\delta}$, where d is the distance between stimulus regions in V1 and depends on the orienta-

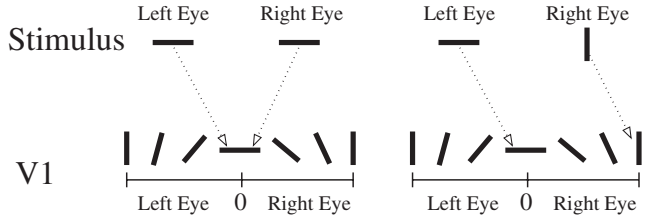

FIG. 1. Mapping of visual stimulus to V1 slice. A bar viewed by the left or right eye drives activity in V1 at a position where the bar orientation matches neural OP (bars) and eye preference. Examples are shown where both eyes view horizontal bars (left) and where the left eye views a horizontal bar and the right eye views a vertical bar (right).

tion difference between left-eye and right-eye stimuli as in Fig. 1, δ is the OP width, and $h_{\max}$ is determined by stimulus strength. The only conditions we impose on $w(R)$ for rivalry are $w(-x) = w(x)$, and $w(R) < 0$ for large R. These are satisfied by a Mexican-hat form commonly used in cortical models: $w(R) = ce^{-R^2/r_1^2} - (r_1/r_2)e^{-R^2/r_2^2}$ with $r_1 < r_2$ and $c > 0$—although excitatory connections in $w(R)$ are unnecessary for rivalry as neural activity can be driven above threshold by the stimulus term in (1).

Extending the analysis in [10] to nonuniform $h(x)$ and $\theta(x, t)$, we set time derivatives in (1) and (2) to zero, and consider an equilibrium comprising N_s spatially localized regions each with $u > \theta$ over width m centered at a_i:

$$u_s(x) = \sum_{i=1}^{N_s} \int_{-m/2}^{m/2} w(x - x' - a_i)dx' + h(x), \qquad (3)$$

$$\theta_s(x) = \theta_0 + \kappa u(x)H(u(x)). \qquad (4)$$

We term these localized states *solitons* [13]: in [14] states similar to those given by (3) were shown to have several particlelike properties, and despite the nonlinearity, dissipation, and external driving present, perturbed equilibrium states always remained localized in numerical simulations of (1) and (2). Consistency requires $u(x) = \theta(x)$ at the boundaries of each localized region, and is implemented using (3) and (4) with $u_s(a_i \pm m/2) > 0$, yielding $2N_s$ simultaneous equations $u_s(a_i \pm m/2) = \theta_0/(1 - \kappa)$. For $N_s = 1$ and $a_1 = 0$, we get $u_s(\pm m/2) = \theta_0/(1 - \kappa)$. Upon using (3) and the symmetry $h(-m/2) = h(m/2)$, this becomes

$$\int_0^m w(x)dx + h\left(-\frac{m}{2}\right) = \frac{\theta_0}{1 - \kappa}, \qquad (5)$$

which is used to determine m. An equilibrium from (3)–(5) is shown in Fig. 2(a).

To determine equilibrium stability we apply an Evans function technique [11], in which linear deviations given by $u(x, t) = u_s(x) + \delta u(x)e^{\lambda t}$ and $\theta(x, t) = \theta_s(x) + \delta\theta(x)e^{\lambda t}$ are substituted into (1) and (2), and an eigenvalue equation is generated by expanding to first order in $\delta u(x)$ and $\delta\theta(x)$. Defining $(x_1, x_2) = (-m, m)/2$ for $N_s = 1$, this

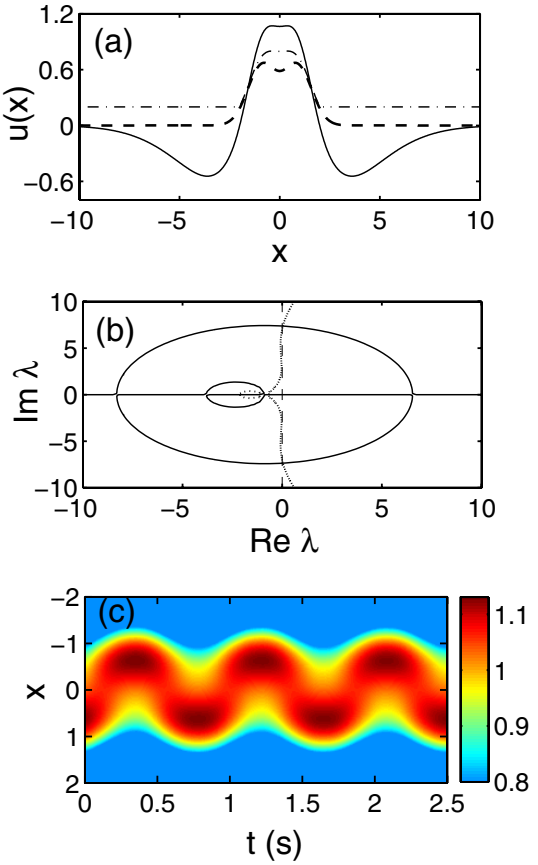

FIG. 2 (color online). Fusion-rivalry transition for $N_s = 1$. (a) Equilibrium u_s (solid line) and θ_s (dash-dotted line) from (3)–(5) for a stimulus (dashed line), and parameters $h_{\max} = 0.64$, $\delta = 1$, $d = 1.77$, $c = 0.7$, $r_1 = 2$, $r_2 = 4.5$, $\theta_0 = 0.2$, and $\kappa = 0.56$. (b) Zeros of $\mathcal{E}(\lambda)$ from (6) with $\tau_f = 20$ ms and $\tau_s = 500$ ms occur at intersections of the solid line and the dotted line. (c) Numerical solution for $u(x, t) > 0.8$ from (1) and (2).

eigenvalue equation can be written as $\mathcal{E}(\lambda) = 0$, with

$$\mathcal{E}(\lambda) = \det\left(\frac{\mathcal{D}_f(\lambda)\mathcal{D}_s(\lambda)}{\mathcal{D}_s(\lambda) - \kappa}\mathcal{I} - \mathcal{A}\right), \qquad (6)$$

where $\mathcal{A}$ is a $2N_s \times 2N_s$ matrix with elements $\mathcal{A}_{ij} = w(x_i - x_j)/|u_s'(x_j) - \theta_s'(x_j)|$, $\mathcal{I}$ is an identity matrix, and $\mathcal{D}_a(\lambda) = \tau_a\lambda + 1$. The derivatives are found from (3) and (4), giving $|u_s'(x_i) - \theta_s'(x_i)| = (1 - \kappa)|w(x_i + m/2) - w(x_i - m/2) + h'(x_i)|$ for $N_s = 1$. Contours of $\mathrm{Re}\mathcal{E}(\lambda) = 0$ and $\mathrm{Im}\mathcal{E}(\lambda) = 0$ are shown in Fig. 2(b) for the $N_s = 1$ equilibrium, and $\mathcal{E}(\lambda) = 0$ where they intersect, corresponding to an eigenvalue of the linear stability problem. For $d < d_c$ ($\simeq 1.77$ in Fig. 2), where d depends on the orientation difference between left-eye and right-eye stimuli as in Fig. 1, we find $\mathrm{Re}\lambda < 0$ so the one-soliton equilibrium is stable. We interpret this as binocular fusion: two monocular stimuli form a stable nonoscillating percept [6]. As d increases, the orientation difference between the two monocular stimuli reaches a critical level at $d = d_c$, where a pair of complex-conjugate eigenvalues cross $\mathrm{Re}\lambda = 0$:

the one-soliton equilibrium is now unstable to a Hopf bifurcation. The numerical solution for $u(x, t)$ is shown in Fig. 2(c), where high neural activity localizes to one stimulus region for approximately 0.5 s before moving to the other stimulus region for approximately 0.5 s, and so on. We interpret this as binocular rivalry: two monocular stimuli lead to oscillations between states where one stimulus is dominant and the other is suppressed [6].

The origin of the Hopf instability for $N_s = 1$ is the following: the coupling term in (2) causes the spiking threshold to increase over time τ_s in the soliton region, resulting in a translational instability as the soliton moves to avoid a region of high threshold. However, a stimulus breaks translational symmetry and tends to pin the soliton. For $d < d_c$, one soliton can span both stimulus regions and so remains centered midway between them. At $d = d_c$, this is no longer the case just off equilibrium, and the soliton must choose one region or the other. As the spiking threshold increases in one region, the soliton eventually moves to the other, as in Fig. 2(c). This is consistent with rivalry as a single soliton that oscillates between two stimulus regions.

To find the $N_s = 2$ equilibrium we assume $(a_1, a_2) = (-a, a)/2$ for $a > 0$, leading to $u_s(\pm a/2 \pm m/2) = \theta_0/(1 - \kappa)$. The stimulus symmetry obeys $h(-a/2 - m/2) = h(a/2 + m/2)$ and $h(-a/2 + m/2) = h(a/2 - m/2)$, reducing the four equations to two. One is

$$\int_0^m [w(x) + w(x + a)]dx + h\left(-\frac{m}{2} - \frac{a}{2}\right) = \frac{\theta_0}{1 - \kappa}, \quad (7)$$

which determines m when a is fixed. Subtracting the remaining equation from (7), yields

$$\int_0^m [w(x + a) - w(x - a)]dx = h\left(\frac{m}{2} - \frac{a}{2}\right) - h\left(-\frac{m}{2} - \frac{a}{2}\right), \quad (8)$$

which determines a when m is fixed. Both (7) and (8) are solved self-consistently. Solitons usually repel due to long-range inhibition, and $a \to \infty$. However, inclusion of a stimulus allows (8) to be solved for finite a, and a resulting equilibrium is shown in Fig. 3(a). Defining $(x_1, x_2, x_3, x_4) = (-m - a, m - a, -m + a, m + a)/2$ generates the previous eigenvalue equation, with $\mathcal{E}(\lambda)$ from (6) and $|u_s'(x_i) - \theta_s'(x_i)| = (1 - \kappa)|w(x_i + m/2 + a/2) + w(x_i + m/2 - a/2) - w(x_i - m/2 + a/2) - w(x_i - m/2 - a/2) + h'(x_i)|$. The two-soliton equilibrium is stable for $d > d_c$ ($\simeq$6.1 in Fig. 3), and we interpret this as binocular fusion. As d decreases, at $d = d_c$ a pair of complex-conjugate eigenvalues cross $\mathrm{Re}\lambda = 0$ in Fig. 3(b) and the two-soliton equilibrium becomes unstable to a Hopf bifurcation. The numerical solution for $u(x, t)$ is shown in Fig. 3(c), where neural activity grows in one stimulus region for approximately 1.5 s, before it decays there and grows in the other stimulus region for approximately 1.5 s, and so on. We interpret this as binocular rivalry.

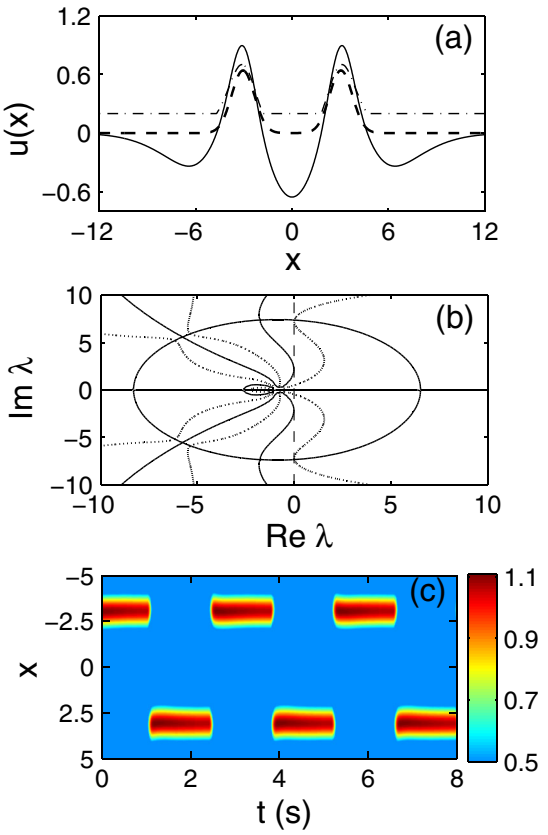

FIG. 3 (color online). Fusion-rivalry transition for $N_s = 2$. (a) Equilibrium u_s (solid line) and θ_s (dash-dotted line) for a stimulus (dashed line) with $d = 6.1$ and other values as in Fig. 2. (b) Zeros of $\mathcal{E}(\lambda)$. (c) Numerical solution for $u(x, t) > 0.5$ from (1) and (2).

The Hopf instability for $N_s = 2$ has a different origin to that for $N_s = 1$. Both stimulus regions are now occupied, so each soliton remains fixed in position. For $d > d_c$, there is only weak reciprocal inhibition between two solitons and both remain above threshold. At $d = d_c$, each soliton inhibits the other more strongly, and just off equilibrium only one can remain above threshold. However, this dominant soliton falls below threshold after τ_s, releasing the suppressed soliton from inhibition. The latter then grows above threshold and becomes dominant, as in Fig. 3(c). This is consistent with rivalry as two solitons, one fixed at each stimulus region, that oscillate out of phase with one another.

Complete dominance of either monocular stimulus is less likely as both stimuli extend over a larger part of V1; instead, rivalry breaks up into a patchwork of zones of alternating dominance [1,2,6]. This can be described in our model by considering an extended 1D slice with spatially periodic OP and eye preference. We take the basic unit cell shown in Fig. 1 and repeat it N times end to end: setting the unit cell length to $L \simeq 2r_2$ based on estimates of $\sim$1 mm unit cell size [5,15], and the $\sim$0.5 mm range of nonspecific lateral connections in V1 [15,16]. As the orientation difference $\Delta\phi$ between two monocular stimuli increases, binocular fusion gives way to binocular rivalry

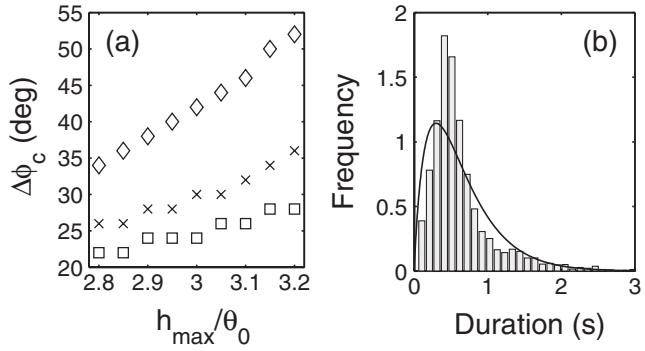

FIG. 4. Model predictions for binocular rivalry with parameters as in Fig. 2. (a) $\Delta\phi_c$ vs $h_{\max}$ for $\delta = 0.8$ (diamonds), $\delta = 1$ (crosses), and $\delta = 1.2$ (squares). (b) Dominance durations from (1) and (2) with added noise and fitted gamma distribution (solid line).

at $\Delta\phi_c = 180°(d_c/L)$, where d_c is the critical value of d for $N_s = 1$. For small $\Delta\phi \geq \Delta\phi_c$, interactions between solitons in neighboring unit cells are weak, so each soliton alternates independently on short time scales. A patchwork forms unless neighboring alternations all begin precisely in phase and the system is noise-free. As $\Delta\phi$ increases, the interactions become stronger, until at $\Delta\phi = 90°$ ($d = L/2$) there is equal reciprocal inhibition between all solitons and the activity in each unit cell is far from the $N_s = 1$ equilibrium. Fusion eventually sets in again as $\Delta\phi \to 180°$ and the orientations are again similar. In Fig. 4(a), $\Delta\phi_c$ is plotted for different values of the stimulus parameters. The results agree with [17], where $\Delta\phi_c$ for fusion-rivalry and rivalry-fusion transitions was 17.1°–30.4°. Figure 4(a) also shows $\Delta\phi_c$ increasing approximately linearly with increase in $h_{\max}$ and decrease in δ. The reason for the δ dependence is that it is less likely one soliton can span two stimulus regions as each region widens, so the soliton becomes unstable at smaller $\Delta\phi_c$. The h dependence is due to the above tendency of a stimulus to pin a soliton. This behavior can be interpreted using the energy (i.e., Lyapunov) function $\mathcal{F}$ of Eq. (1), which has a stimulus-dependent part given by $\mathcal{F}_{\text{stim}} = -\langle h, H(u_s - \theta_s)\rangle$, where $\langle f, g\rangle$ is the inner product of functions f and g [14]. This means that energy is minimized in regions of soliton-stimulus overlap where h is maximal, so increasing h stabilizes a soliton—raising $\Delta\phi_c$ in Fig. 4(a). In [17], a lower stimulus contrast led to larger $\Delta\phi_c$, meaning that $h_{\max}$ should be inversely related to stimulus contrast. This interpretation is supported by [18], where decreasing the contrast of one stimulus corresponded to a decrease in $\mathcal{F}$ (i.e., by increasing h) of the opposite stimulus, thereby lengthening its dominance duration—as found experimentally [1,2,18]. In our model, $\Delta\phi_c$ is therefore determined by OP periodicity and the range of lateral connections in V1, as well as specific stimulus attributes.

A histogram of stimulus dominance durations simulated from (1) and (2) with added noise is shown in Fig. 4(b). Specifically, we added $+1.5$ or -1.5 with equal probability to the right-hand side of (2) at each time step and each grid point. Each time u crossed $\theta \pm \Delta\theta$ (where $\pm\Delta\theta$ was used to ensure a definite switch in dominance had taken place) at a point chosen near the stimulus maximum, the time since the previous crossing was recorded. A total of 3137 crossings were simulated. A gamma distribution $\beta^\alpha x^{\alpha-1} e^{-\beta x}/\Gamma(\alpha)$ was fitted to the histogram in Fig. 4(b) by matching the mean and variance of both, giving $\alpha = 1.9$ and $\beta = 2.9$. These values are well within the ranges $\alpha = 1.3$–6.7, and $\beta = 0.46$–4.0 from fits to experimental and simulated distributions [6,7,9].

In summary, we have developed a soliton model that gives the first theoretical prediction of binocular rivalry onset. It also predicts two types of competitive neural dynamics consistent with rivalry and matches experimental results, including stimulus conditions for rivalry onset and the distribution of dominance durations.

The Australian Research Council supported this work.

[1] R. Blake, Psychol. Rev. **96**, 145 (1989).
[2] R. Blake and N. K. Logothetis, Nat. Rev. Neurosci. **3**, 13 (2002).
[3] A. Polonsky, R. Blake, J. Braun, and D. J. Heeger, Nat. Neurosci. **3**, 1153 (2000).
[4] S. H. Lee, R. Blake, and D. J. Heeger, Nat. Neurosci. **8**, 22 (2005).
[5] N. V. Swindale, Netw., Comput. Neural Syst. **7**, 161 (1996).
[6] S. R. Lehky, Perception **17**, 215 (1988).
[7] H. R. Wilson, B. Krupa, and F. Wilkinson, Nat. Neurosci. **3**, 170 (2000).
[8] H. R. Wilson, R. Blake, and S. H. Lee, Nature (London) **412**, 907 (2001).
[9] C. R. Laing and C. C. Chow, J. Comput. Neurosci. **12**, 39 (2002).
[10] S. Amari, Biol. Cybern. **27**, 77 (1977).
[11] S. Coombes and M. R. Owen, Phys. Rev. Lett. **94**, 148102 (2005).
[12] P. N. Loxley and P. A. Robinson, Biol. Cybern. **97**, 113 (2007).
[13] R. Rajaraman, *Solitons and Instantons* (North-Holland, Amsterdam, 1982).
[14] P. N. Loxley and P. A. Robinson, Phys. Rev. E **76**, 046224 (2007).
[15] W. H. Bosking, Y. Zhang, B. Schofield, and D. Fitzpatrick, J. Neurosci. **17**, 2112 (1997).
[16] R. Malach, Y. Amir, M. Harel, and A. Grinvald, Proc. Natl. Acad. Sci. U.S.A. **90**, 10 469 (1993).
[17] A. Buckthought, J. Kim, and H. R. Wilson, Vision Res. **48**, 819 (2008).
[18] Y. J. Kim, M. Grabowecky, and S. Suzuki, Vision Res. **46**, 392 (2006).